J. Chem. Sci., Vol. 118, No. 1, January 2006, pp. 47–55.

Design and fabrication of an automated temperature programmed reaction system to evaluate 3-way catalysts $Ce_{1-x-y}(La/Y)_xPt_yO_{2-d}$

ARUP GAYEN,[a] TINKU BAIDYA,[a] G S RAMESH,[b] R SRIHARI[a] and M S HEGDE[a,*]

[a]Solid State and Structural Chemistry Unit, Indian Institute of Science, Bangalore 560 012
[b]Techno Science Instruments, Bangalore 560 021
e-mail: mshegde@sscu.iisc.ernet.in

Abstract. A completely automated temperature-programmed reaction (TPR) system for carrying out gas–solid catalytic reactions under atmospheric flow conditions is fabricated to study CO and hydrocarbon oxidation, and NO reduction. The system consists of an all-stainless steel UHV system, quadrupole mass spectrometer SX200 (VG Scientific), a tubular furnace and micro-reactor, a temperature controller, a versatile gas handling system, and a data acquisition and analysis system. The performance of the system has been tested under standard experimental conditions for CO oxidation over well-characterized $Ce_{1-x-y}Pt_x(La/Y)_yO_{2-d}$ catalysts. Testing of 3-way catalysis with CO, NO and C_2H_2 to convert to CO_2, N_2 and H_2O is done with this catalyst which shows complete removal of pollutants below 325°C. Fixed oxide-ion defects in Pt substituted $Ce_{1-y}(La/Y)_yO_{2-y/2}$ show higher catalytic activity than Pt ion-substituted CeO_2.

Keywords. Automatic TPR; ceria, three way catalysis.

1. Introduction

Temperature-programmed desorption (TPD) is one limit of a more general technique, temperature programmed reaction (TPR). Since the design of the first desorption system by Cvetonovic and Amenomiya,[1] the technique has become indispensable for probing gas-solid interface in heterogeneous catalysis.[2–9]

TPD analysis permits identification of the strength, number and type of active sites available on the catalyst surface. The technique consists in desorbing, by a linear temperature rate, a reactive gas previously chemisorbed on the surface. When the test gas saturates the active sites, a linear temperature ramp is applied to the reactor. At a certain temperature, the heat overcomes the activation energy of the gas/solid system, therefore breaking the bond between the active site and the chemisorbed molecule. Flow of an inert gas carrier (typically argon, nitrogen or helium) is used to transport the gas molecules desorbed from the catalyst surface at different temperatures, and the amount is monitored by a mass spectrometer as a function of temperature. The plot of the mass peak intensity versus temperature is termed a thermogram or a TPD profile. The same system can be employed to carry out a temperature-programmed reaction (TPR) where variation of concentrations of the reactants and products is monitored as a function of temperature. The corresponding profile is called a TPR profile.

Here we report the design and fabrication of a temperature-programmed reaction system and its performance for low temperature CO oxidation and 3-way catalytic test over $Ce_{1-x-y}Pt_x(La/Y)_yO_{2-d}$ catalysts synthesized by a single-step solution combustion method.

2. Design and fabrication

The first comprehensive and automated TPR system was fabricated by Boer *et al*[10] in 1982 employing a thermal conductivity detector (TCD) for the identification and quantification of the product gases. The present system employs a quadrupole mass spectrometer for reactant/product analysis, which is a very fast technique.[11] Figure 1 shows a block diagram of the set-up fabricated to study gas–solid heterogeneous catalytic reactions under atmospheric flow conditions. A brief description of each of the subsystems is presented.

2.1 *Vacuum system*

The set-up consists of two vacuum systems, one is an ultra-high vacuum system (UHV) and the other is

Dedicated to Prof J Gopalakrishnan on his 62nd birthday
*For correspondence

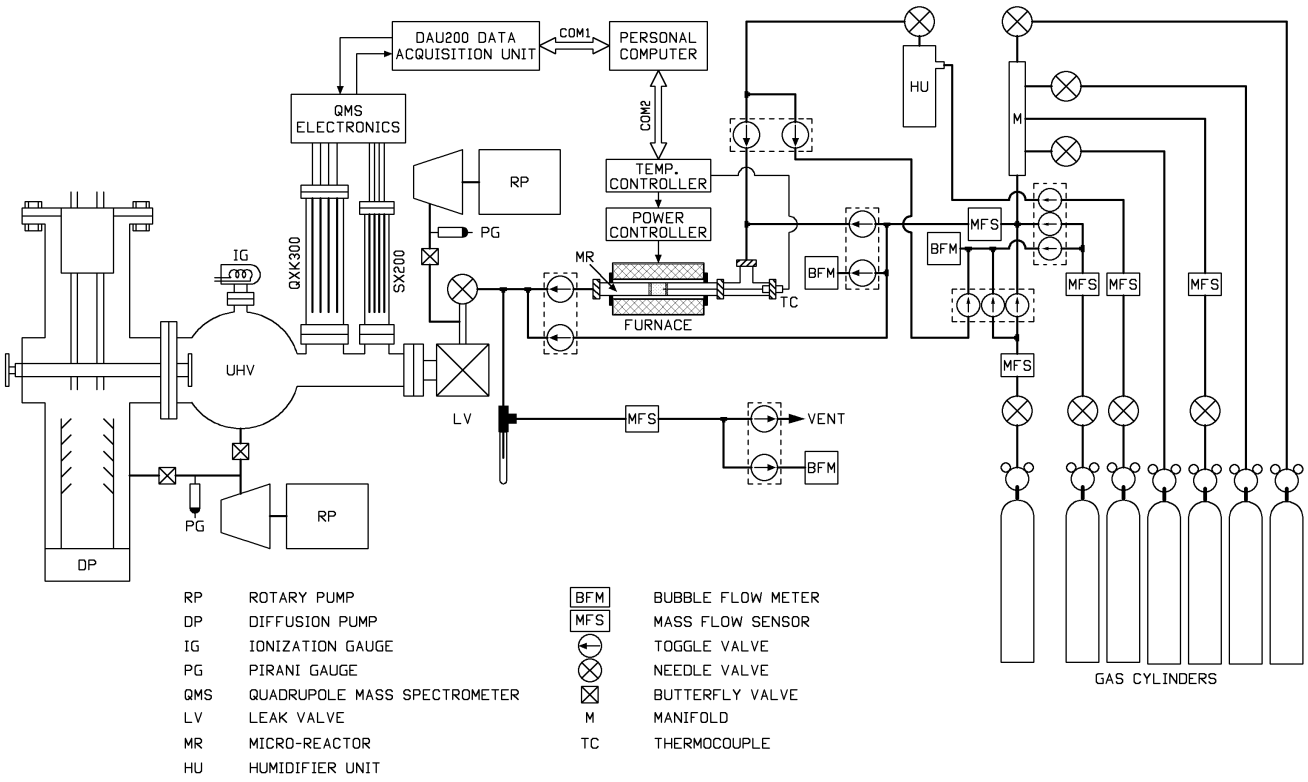

Figure 1. Schematic diagram of the TPR/TPD system fabricated.

a high vacuum (HV) system. The UHV system produces a vacuum of ~10^{-8} Torr with a 4″ Edwards Santovac oil diffusion pump and a rotary pump fitted with a liquid nitrogen trap. The multi-port stainless steel UHV chamber houses the quadrupole mass spectrometer (QMS) mounted on a port perpendicular to the flow of the leaked gases at a distance of ~5 cm for analysis along with a fine control leak-in UHV valve and an ionization gauge. The vacuum is continuously monitored by the ionization gauge. The system is backed by UPS power to run the experiment without interruption. A separate high vacuum (~10^{-5} Torr) system with a diffusion pump/rotary pump is set up for sampling the product gases. Differential pumping is required to remove the dead-volume generated through continuous sampling from the needle valve at the outlet line from the micro-reactor of the gas-handling system and the leak-in valve to the QMS chamber connected through a “T” joint.

2.2 *Mass spectrometer*

A VG QMS instrument, model SX200 has been employed for the analysis of product gases. The SX200 has a twin-filament ion source and dual detectors selectable between faraday cup and channel electron multiplier. With an electron multiplier as the detector, the time response of a mass spectrometer is of the order of nanoseconds, enabling the system to differentiate and detect the masses of the gaseous products almost instantaneously.

2.3 *Gas-handling system*

A versatile gas-handling system has been built to pass carrier and reactant gases so as to obtain a gas mixture of the desired composition. For this purpose, ultra-high pure as well as calibrated gas mixtures were obtained from Bhuruka Gases Limited, Bangalore. All the gas lines are made of 1/8 or 1/16 inch stainless steel (ss) tubes to avoid any corrosion due to the use of gases like nitric oxide. Each gas line starts with a gas cylinder with a pressure regulator followed by a needle valve (Hind High Vacuum, Bangalore), a mass flow sensor and three toggle valves, the opening of which allows the gas to flow either through the micro-rector containing catalyst or through the by-pass line, or is passed through the bubble flowmeter. The needle valve controls the gas flow; the mass flow sensor measures the gas flow in

millilitres per minute (mostly represented as SCCM, standard cubic centimetre per minute) to a precision of 0·2 sccm. The gases are mixed in a manifold prior to entering the quartz micro-reactor. The flow can be measured before as well as after entry into the catalyst bed. This is a necessary requirement to decide whether there is any pressure drop due to blockage in the catalyst bed.

The flowmetre is an essential constituent of any flow system. We procured two types of mass airflow sensors, namely Bronkhorst Hi Tech BV and AWM3100V, for this purpose. Whereas the former sensor has the capability to measure flow in the range 0–500 sccm, the latter can sense it in the range 0–200 sccm. The micro-switch AWM3100V micro-bridge mass airflow sensor was obtained from Tata Honeywell Company. These sensors have built-in amplifiers to amplify the bridge signal to a level of 5 V. For calibration purposes, a standard bubble flow-metre from Mayura Analytical Private Ltd., Bangalore, was employed. The flow was found to be linear in the 0–100 sccm ranges, the region where most studies are usually carried out. The Bronkhorst Hi Tech BV sensor, situated after the manifold and before the toggle valve, was used to measure the total flow.

Two parameters of interest in plugged-flow reactors are the gas hourly space velocity (GHSV) and the contact time (t). The GHSV is defined as the volume of gases flowing per unit volume of the catalyst bed per hour. It is expressed as, GHSV = F_t/V, where F_t is the total flow (in ml h^{-1}) and V is the volume of the catalyst bed (in ml). Thus, the unit of GHSV is h^{-1}. The contact time (expressed as $t = w/F_t$) is the residence time of the reactant on the catalyst surface for it to react. The unit of t is g s cm^{-3}. Typically, 50–200 sccm is the total gas flow and GHSV ~ 25000–50000 h^{-1} is maintained during the reaction.

2.4 *Heating system*

Several factors influence the design and fabrication of an appropriate laboratory test reactor, principles of which have been reviewed by Doraiswamy and Tajbl[12] and mass balance in such reactors has been discussed by Thomas.[13] The heating system employed in our system comprises a tubular furnace, a micro-reactor, a temperature programmer cum controller and a furnace power controller. The miniature tubular furnace, which consumes about a one kilowatt power, has a tubular ID (inner diameter) of 16 mm and length 200 mm. A quartz tube of 6 mm OD (outer diameter) and length 250 mm was used as the micro-reactor and is housed inside the tubular furnace in such a manner as to have a uniform gap around it to facilitate uniform heat transfer. This ensures uniformity of temperature throughout the catalyst bed. The catalyst is placed inside the quartz micro-reactor with its ends plugged with ceramic wool. For free flow of gases, the samples are taken in the form of mesh and when necessary are mixed with silica mesh to get the desired bed length, thereby getting different contact time of the adsorbate and hence different gas hourly space velocity. The micro-reactor can be heated up to 800°C with a uniform heating rate for carrying out catalytic reactions in a carrier gas, usually He, at atmospheric pressure. The furnace temperature can be programmed and controlled using Eurotherm temperature programmer, model 2416. The important parameters such as the start and the end temperature (T1 and T2), rate of heating in deg min^{-1}, and duration are set before each experiment and the commencement of reaction is monitored by a software program through PC via RS232 interface. Typical heating rates range from 5°C min^{-1} to 15°C min^{-1}.

2.5 *Data acquisition and control system*

The data acquisition and control system (DAS) is responsible for controlling the mass scan and acquiring the mass intensity data into the PC. The temperature data is separately acquired by the PC through another serial interface. A versatile DAS model DAU200 has been designed and fabricated for this purpose.

The DAS consists of the spectrometer controller input and output signals (from SX200 QMS controller), namely Y-signal output and external X-scan input, a data acquisition unit (DAU200), a serial interface (RS232) and an IBM compatible personal computer. The DAU200 comprises a 12-bit ADC (analog to digital converter) and a 12-bit DAC (digital to analog converter), which are serially interfaced to a micro-controller. The DAC generates the required scan voltage to scan the mass spectrometer at selected mass range and scan rate. The temperature is sensed by another serial port.

2.6 *QMS_Soft software program*

A completely Windows-based and very user-friendly software program to scan and acquire data from the

spectrometer and temperature controller has been developed using Visual Basic 6·0. The selectable options from the menu bar are Instrument, Experiment, Interface and Data Analysis. There are two modes/varieties of experiments one can do. The first is the "continuous TPR", which involves continuous programming of temperature, and the second is the "isotemp TPR" for constant temperature reaction. In continuous TPR mode, various parameters can be defined such as the mass range, starting and ending temperatures T1, T2, heating rate, scan rate, and the output file name. Each scan is on-line plotted and stored into a random access file as a RAW file. In the analysis mode, any file can be loaded and the raw data can be plotted, where the user can see each scan. Finally, the required number of peaks can be selected to generate thermograms (PKS files). The plot of the intensity of each mass as a function of temperature is known as a thermogram and the plot of all these thermograms is known as a TPR plot or profile. Further, the data can be exported in ASCII format for further analysis and calculation. In the constant temperature mode, all the scans are averaged to a single data file for analysis. The concentrations of the different species are obtained by dividing the observed intensities by the corresponding ionization cross section.

2.7 *TPR and spectrometer operation*

The reaction gas mixture of desired composition and flow rate is monitored through the flowmetres, using He as the carrier gas, and passed through the quartz micro-reactor, which is to be subsequently heated. The mass spectrometer controller is adjusted with proper settings on the emission control, mass range, scan rate etc. to obtain a mass scan on the oscilloscope. A small fraction of the gaseous reactants and/product stream coming out of the micro-reactor at atmospheric pressure (760 Torr) is leaked to the high vacuum unit at a pressure of about 0·2 Torr by the needle valve and the rest of the stream goes to the atmosphere through the vent line. The 1/16″ SS tube carrying the output gas is taken close to the needle of the leak valve so that the dead volume is reduced to less than 0·2 cc. At a flow rate of 1·6 cc/s (100 sccm), the dead volume gas is replaced 8 times in a second. From this volume, the gas is leaked to the mouth of the second fine leak-in valve (VG MD95) by using a 1 mm bore capillary and the total volume of this chamber is less than 2 cc. This second 2 cc chamber is pumped by a diffusion pump to 10^{-5} Torr by a 200 l/min diffusion pump coupled to a rotary pump. When the output gas is leaked, the pressure in the chamber to fine leak-in valve rises from 10^{-5} Torr to 0·015 Torr ($p_{gas}/p_{residual\ gas}$ = 1500) and the back pressure in the rotary from 0·01 to 0·2 Torr. From the MD95 VG valve, output gas is leaked to the mass analyser chamber to a vacuum from 10^{-8} to 10^{-6} Torr from 2 cc volume 0·015 Torr. Thus, within a second, the gases leaving the reaction zone are detected. With a heating rate of 10°/min, rise in temperature is less than 0·2° in the reactor. Thus, by using a differential pumping method, we have overcome the problem of dead volume and also the use of a capillary for sampling. Finally, the system is tested by actually injecting O_2 (m/z = 32 mass) to He flow (100 sccm) at the reaction zone and in just 1 s, the O_2 mass peak is observed in the QMS. The selected mass range, as a function of temperature, is acquired by the computer interface module and stored into a file in the PC. Simultaneously, each scan is displayed on the screen. The analysis option is then selected to read the data file. File parameters such as total number of scans, T1, T2 etc. are displayed. Mass peaks can be selected by entering the mass numbers. The thermograms (mass peak intensity vs. temperature) are then generated and stored as PKS files (the file names end with the respective mass numbers). These PKS files can be viewed using plot thermogram option (one file at a time) or TPR plot (all the PKS files generated for one single experiment). For complete analysis, these ASCII files are imported in Origin and plotted to get derived results like percent conversion, rate etc. Photograph of the TPR system is given in figure 2.

2.8 *Synthesis and characterization of catalysts*

The $Ce_{1-x}Pt_xO_{2-d}$ (x = 0·01) catalyst was prepared by the combustion of a stoichiometric aqueous mixture of $(NH_4)_2Ce(NO_3)_6$, H_2PtCl_6 and ODH as reported earlier.[14] For the preparation of lanthanum- and yttrium-substituted $Ce_{1-x}Pt_xO_{2-d}$, stoichiometric amounts of the corresponding oxides, La_2O_3 and Y_2O_3, were dissolved in minimum volume of dilute HNO_3 solution followed by evaporation to dryness to get the nitrate precursor, in which $(NH_4)_2Ce(NO_3)_6$, H_2PtCl_6 and ODH were added, dissolved in ~30 ml of distilled water and the mixture was subjected to combustion at ~350°C to get the required catalyst composition. We have studied the effect of 10 atom% each of La

Figure 2. TPR instrument for catalysis studies.

and Y substitution in CeO_2 along with 1 atom% Pt on the structure and CO oxidation activity.

XRD of the prepared catalysts was recorded on a Philips X'Pert diffractometer at a scan rate of 0·5° min^{-1} with 0·02° step size in the 2*q* ranges 20 to 80°. The structure was refined using the FullProf-fp2k program.[15] The number of parameters refined simultaneously was 19.

XPS of the samples were recorded in an ESCA-3 Mark II spectrometer (VG Scientific Ltd., England) using AlK*a* radiation (1486·6 eV). Binding energies were corrected from charge effects by reference to the C(1*s*) peak of carbon contamination at 285 eV and measured with a precision of ± 0·2 eV.

3. Results and discussion

3.1 *XRD studies*

Powder XRD patterns of the catalysts were recorded to see the nature of Pt phases on increasing the Pt content. Detailed structural study on $Ce_{0·99}Pt_{0·01}O_{2-d}$ can be found in ref. (14). The ions La^{3+} and Y^{3+} can be substituted for Ce^{4+} ion in the fluorite structure forming $Ce_{1-y}(La/Y)_yO_{2-y/2}$. Thus, oxide-ion vacancies can be created. To see Pt dispersion behaviour in presence of La and Y, we prepared 1 atom% Pt/$Ce_{1-y}(La/Y)_yO_{2-y/2}$. Peaks due to either La_2O_3 or Y_2O_3 are not observed. Thus, there is formation of a solid solution of $Ce_{1-y}(La/Y)_yO_{2-y/2}$.

The XRD patterns were Rietveld refined considering the solid solution model $Ce_{1-x-y}Pt_x(La/Y)_yO_{2-d}$ (x = 0·01; y = 0·1). The fit is good with negligible residual background. Figures 3a and b show the Rietveld refined patterns of as-prepared catalysts of 1 atom% Pt in $Ce_{0·9}La_{0·1}O_{1·95}$ and $Ce_{0·9}Y_{0·1}O_{1·95}$, respectively. The refined parameters are listed in table 1. The lattice parameter a increases from 5·4156(8) Å in $Ce_{0·99}Pt_{0·01}O_{2-d}$ to 5·4415(7) Å on La^{3+} substitution and a = 5·4111(9) Å on Y^{3+} substitution. This is expected since the ionic radius of La^{3+} (1·16 Å) is higher than that of Ce^{4+} (0·97 Å) and the radius of Y^{3+} (1·02 Å) is closer to cerium. On Rietveld refinement, the compositions obtained are $Ce_{0·99}Pt_{0·01}O_{1·88(4)}$, $Ce_{0·89}Pt_{0·01}La_{0·10}O_{1·85(3)}$ and $Ce_{0·89}Pt_{0·01}Y_{0·10}O_{1·90(4)}$. Clearly, oxide vacancies are formed due to La^{3+} and Y^{3+} ion substitution for Ce^{4+}.

3.2 *XPS studies*

A detailed XPS study of $Ce_{0·99}Pt_{0·01}O_{2-d}$ can be found in ref. (14). In brief, the Pt(4*f*) region shows peaks due to multiple oxidation states. The Pt(4*f*) spectra are much broader than the Pt metal indicat-

Table 1. Rietveld refined parameters for $Ce_{0·99}Pt_{0·01}O_{2-d}$ and 1 atom% Pt in $Ce_{0·9}(La/Y)_{0·1}O_{1·95}$ catalysts.

Catalyst	a (Å)	R_{Bragg}	R_F	R_P	Occ*
$Ce_{0·99}Pt_{0·01}O_{2-d}$	5·4156 (8)	0·866	0·675	5·63	1·88 (4)
1% $Pt/Ce_{0·9}La_{0·1}O_{1·95}$	5·4415 (7)	0·769	0·933	5·48	1·85 (3)
1% $Pt/Ce_{0·9}Y_{0·1}O_{2-d}$	5·4111 (9)	1·03	1·04	6·42	1·90 (4)

*Oxide-ion occupancy

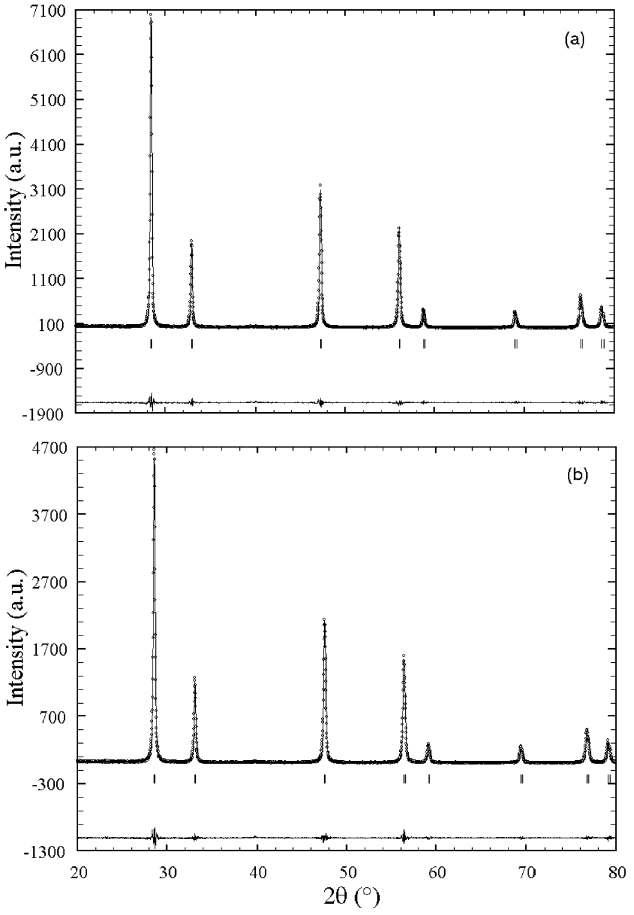

Figure 3. Observed (O), calculated (–) and difference XRD patterns of (**a**) 1 atom% $Pt/Ce_{0·9}La_{0·1}O_{1·95}$ and (**b**) 1 atom% $Pt/Ce_{0·9}Y_{0·1}O_{1·95}$ catalysts. The vertical bars represent Bragg positions.

ing mixed valency of Pt. The Pt($4f_{7/2;5/2}$) peaks at 71·0, 74·2; 71·9, 75·1 and 74·5, 77·7 eV has been assigned to Pt^0, Pt^{2+} and Pt^{4+} states respectively. Thus, Pt is found to be dispersed mostly in 2+ (71%) and 4+ (22%) oxidation states on CeO_2 crystallites with only 7% Pt present as Pt^0 state. If the curves are resolved into only two sets of Pt($4f$) peaks for Pt^{2+} and Pt^{4+}, full width at half maximum (FWHM) of Pt^{2+} peaks becomes too high (3·3 eV), which is nonphysical. Therefore, a trace amount of Pt metal (Pt^0) is taken into account in XPS analysis. The XRD studies of $Ce_{0·99}Pt_{0·01}O_{2-d}$ indicate presence of 0·08% Pt out of 1 atom% Pt taken in the preparation to be Pt metal. XPS shows about 7% Pt in Pt^0 state. Thus, XPS analysis agrees well with the XRD studies.

Figure 4 presents the Pt($4f$) region of 1 atom% $Pt/Ce_{0·9}(La/Y)_{0·1}O_{1·95}$. Accordingly, the doublets at 71·2, 74·4; 72·4, 75·7 and 74·8, 78·1 eV for 1 atom% $Pt/Ce_{0·9}La_{0·1}O_{1·95}$ (Figure 4a) could be assigned to Pt^0 (4%), Pt^{2+} (70%) and Pt^{4+} (26%) oxidation states respectively. The Pt($4f$) peak positions of 1 atom% $Pt/Ce_{0·9}Y_{0·1}O_{1·95}$ (Figure 4b) are at the same positions as that of 1 atom% $Pt/Ce_{0·9}La_{0·1}O_{1·95}$. Unlike $Ce_{0·99}Pt_{0·01}O_{2-d}$, the Pt^{2+} binding energy of the La- and Y-substituted catalysts is higher by ~0·6 eV. The binding energies, FWHM's and relative intensities of different Pt species as observed from the deconvoluted P($4f$) spectra of $Ce_{0·99}Pt_{0·01}O_{2-d}$ and 1 atom% $Pt/Ce_{0·9}(La/Y)_{0·1}O_{1·95}$ catalysts are summarized in table 2. The Pt($4f$) spectra therefore suggest that in La and Y substituted CeO_2, Pt is more ionic than in pure CeO_2. Since La^{3+} and Y^{3+} are more acidic ions, stabilization of Pt in the ionic state is facilitated.

The Ce($3d$) peaks (not shown) of all the samples of $Ce_{0·99}Pt_{0·01}O_{2-d}$ and $Pt/Ce_{1-y}(La/Y)_yO_{2-y/2}$ show characteristic spectra with satellite features. The Ce($3d_{5/2;3/2}$) doublet was observed at 882·9 eV and 901·3 eV, which correspond to CeO_2 with Ce in the 4+ oxidation state. The La($3d$) spectra with characteristic satellites centred 4 eV below the main peak corresponds to La in 3+ oxidation state as observed for pure La_2O_3. The Y($3d$) peak in 1 atom% $Pt/Ce_{0·9}Y_{0·1}O_{1·95}$ was centred at 158 eV, which corresponds to Y in 3+ oxidation state. From the XRD and XPS studies, the catalysts are represented as $Ce_{0·89}La_{0·1}Pt_{0·01}O_{2-d}$ and $Ce_{0·89}Y_{0·1}Pt_{0·01}O_{2-d}$ fluorite phases.

3.3 *CO oxidation activity*

The oxidation of CO by O_2 was used as the probe reaction to test the performance of the TPR system.

Table 2. Binding energies, FWHM's and relative intensities of different Pt species as observed from the deconvoluetd Pt(4*f*) spectra of $Ce_{0·99}Pt_{0·01}O_{2-d}$ and 1 atom% Pt in $Ce_{0·9}(La/Y)_{0·1}O_{1·95}$ catalysts.

Catalyst	Pt species	Binding energy of $4f_{7/2}$ (eV)	FWHM (eV)	Relative intensity (%)
$Ce_{0·99}Pt_{0·01}O_{2-d}$	Pt^0	71·0	2·5	7
	Pt^{2+}	71·9	3·0	71
	Pt^{4+}	74·5	3·3	22
1% $Pt/Ce_{0·9}La_{0·1}O_{1·95}$	Pt^0	71·2	2·4	4
	Pt^{2+}	72·4	2·6	69·5
	Pt^{4+}	74·8	3·1	26·5
1% $Pt/Ce_{0·9}Y_{0·1}O_{1·95}$	Pt^0	71·1	2·4	5·5
	Pt^{2+}	72·4	2·8	69
	Pt^{4+}	74·8	3·1	25·5

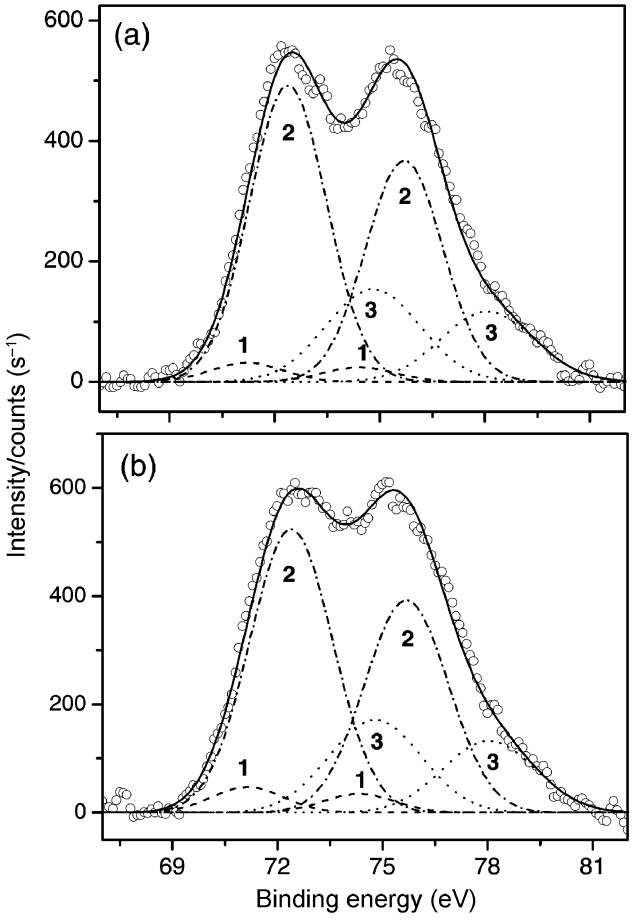

Figure 4. Pt(4f) core-level region in (**a**) 1 atom% Pt/$Ce_{0·9}La_{0·1}O_{1·95}$ and (**b**) 1 atom% $Pt/Ce_{0·9}Y_{0·1}O_{1·95}$ catalysts. The spin-orbit doublets denoted as 1, 2 and 3 correspond to Pt^0, Pt^{2+} and Pt^{4+} oxidation states respectively.

Figure 5 shows the TPR profile for the CO oxidation by O_2 under stoichiometric condition (2 vol.% CO and 1 vol.% O_2) over $Ce_{0·99}Pt_{0·01}O_{2-d}$. The total flow was kept fixed at 100 sccm to achieve a GHSV of 43000 h^{-1}. When the reaction starts, the intensity due to CO (m/z = 28) and O_2 (m/z = 32) decreases and there occurs a simultaneous increase in intensity due to CO_2 (m/z = 44) formation. Thus, the CO oxidation starts at 175°C and is complete beyond 245°C. The light-off temperature (temperature at 50% conversion, T_{50}) is 230°C.

The rate of CO oxidation is calculated from the CO_2 formation rate using the following relation under differential reaction condition:[18]

$$\text{rate} = FX/nw, \tag{1}$$

where F is the inlet flow rate of the reactant CO, X is the fractional conversion at a particular temperature, n is the stoichiometric coefficient and w is the amount of catalysts utilized. The rate is expressed as $m$mol g^{-1} s^{-1}. Actual rate from this equation can be obtained from the slope of W/F_{CO} vs % conversion plots. Indeed, for CO conversion less than 15%, W/F_{CO} varies linearly with % conversion. Below 15% conversion, rates are not influenced by mass transfer and diffusion processes. Further, apparent activation energies (ln(rate) vs $1/T$) are indicative of activity of catalysts when rates are taken below 15% conversion.

The CO oxidation activity is tested over $Ce_{0·89}(La/Y)_{0·10}Pt_{0·01}O_{2-d}$. The percentage CO conversion along with the CO_2 formation rate over these three catalysts is shown in figure 6. Activation energies are lower for La- and Y-substituted CeO_2. Higher catalytic activity of La- and Y-substituted catalysts over Pt/CeO_2 can be explained on the basis of the involvement of defect-mediated mechanism of CO oxidation.[16] CO adsorption takes place preferen-

tially on the Pt^{2+} sites; the area required for the dissociative adsorption of O_2 is eight times the area required for the linear adsorption of CO.[17] Oxide-ion vacancies may thus provide additional sites for oxygen adsorption. The rate-determining step is the dissociation of molecular oxygen and not the adsorption of carbon monoxide. In the La- and Y-substituted catalysts, the presence of more oxide-ion defect facilitates dissociative adsorption of O_2 because oxide-ion defects are the natural sites for oxygen chemisorption. Apart from this, the higher percentages of the ionic component of platinum in 1 atom% $Pt/Ce_{0·9}La_{0·1}O_{1·95}$ (~96%) and 1 atom% $Pt/Ce_{0·9}Y_{0·1}O_{1·95}$ (~94·5%) than in $Ce_{0·99}Pt_{0·01}O_{2-d}$ (~93%) also contribute to the oxide-ion defect formation. That the oxide-ion vacancy is indeed present is shown from the XRD studies.

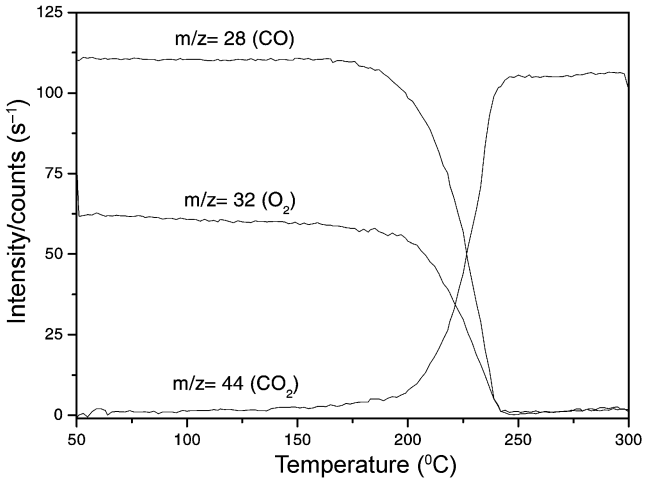

Figure 5. TPR profile for CO oxidation by O_2 over $Ce_{0·99}Pt_{0·01}O_{2-d}$ catalyst. Reaction conditions: CO = 2 vol.%, O_2 = 1 vol.%, Total flow = 100 sccm, GHSV = 43000 h^{-1} and w = 150 mg.

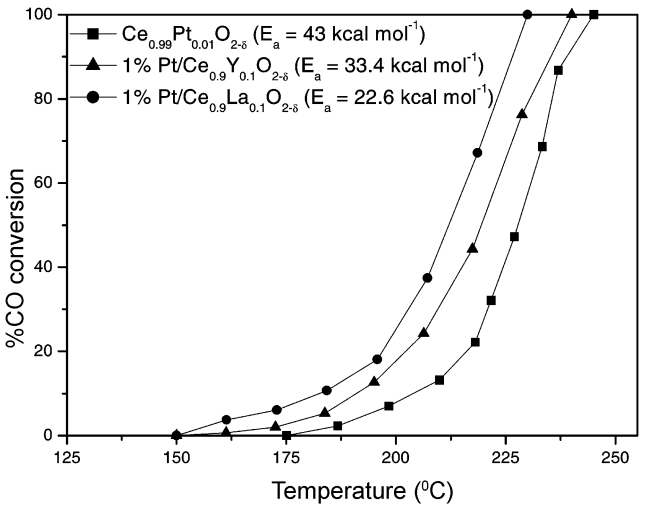

Figure 6. %CO conversion and corresponding rates for CO + O_2 reaction on (**a**) $Ce_{0·99}Pt_{0·01}O_{2-d}$, (**b**) 1 atom% $Pt/Ce_{0·9}La_{0·1}O_{1·95}$ and (**c**) 1 atom% $Pt/Ce_{0·9}Y_{0·1}O_{1·95}$. Reaction conditions: CO = 2 vol.%, O_2 = 1 vol.%, total flow = 100 sccm, GHSV = 43000 h^{-1} and w = 150 mg.

Based on the solid solution model of the catalyst samples studied here, the redox mechanism for CO oxidation by O_2 is presented in the following scheme:

$$\tfrac{1}{2}O_2 + V_{O^{2-}}^{\bullet\bullet} \rightarrow O_o^x + 2h^{\bullet}$$

$$(+\ Ce^{4+}\text{–}O\text{–}Pt^{2+}\text{–}) + CO + O_0^x \rightarrow (\text{–}Ce^{4+}\text{–}O\text{–}Pt^{0}\text{–}) + V_{O^{2-}}^{\bullet\bullet} + CO_2\uparrow$$

$$(\text{–}Ce^{4+}\text{–}O\text{–}Pt^{0}\text{–}) + h^{\bullet} \rightarrow (\text{–}Ce^{3+}\text{–}O\text{–}Pt^{2+}\text{–})$$

$$(\text{–}Ce^{3+}\text{–}O\text{–}Pt^{2+}\text{–}) - + h^{\bullet} \rightarrow (\text{–}Ce^{2+}\text{–}O\text{–}Pt^{2+}\text{–})$$

$$\tfrac{1}{2}O_2 + CO \rightarrow CO_2$$

Where $V_{O^{2-}}^{\bullet\bullet}$, O_o^x and $h^{\bullet}$ are doubly ionized oxide-ion vacancy, neutral oxygen occupied in the vacancy and electron hole respectively. The vacancy $V_{O^{2-}}^{\bullet\bullet}$ is higher for La- and Y-substituted catalysts and hence they are expected to dissociate oxygen more easily. This is reflected in higher activity of these catalysts over pure Pt ion-substituted CeO_2 catalyst. The more general way to present conversion efficiency is the turnover frequency, which is the rate ($m$mol g^{-1} s^{-1}) divided by the active site concentration ($m$mol g^{-1}) and is expressed as s^{-1}. The total metal concentration was taken as the measure of active site concentration. The rate and TOF over $Ce_{0·99}Pt_{0·01}O_{2-d}$ and 10 atom% La- and Y-substituted $Ce_{0·99}Pt_{0·01}O_{2-d}$ catalysts are listed in table 3. Note that the rate and TOF are

Table 3. Rate and turnover frequency (TOF) of CO + O_2 reaction over different catalysts at different temperatures.

Catalyst	Rate ($m$mol g^{-1} s^{-1})	TOF (s^{-1})
$Ce_{0·99}Pt_{0·01}O_{2-d}$	NR (160°C)	NR (160°C)
	NR (170°C)	NR (170°C)
	0·12 (180°C)	0·002 (180°C)
1% $Pt/Ce_{0·9}La_{0·1}O_{1·95}$	0·36 (160°C)	0·006 (160°C)
	0·57 (170°C)	0·01 (1700°C)
	0·92 (180°C)	0·016 (180°C)
1% $Pt/Ce_{0·9}Y_{0·1}O_{1·95}$	0·10 (160°C)	0·002 (160°C)
	0·20 (170°C)	0·003 (170°C)
	0·46 (180°C)	0·008 (180°C)

NR – no reaction

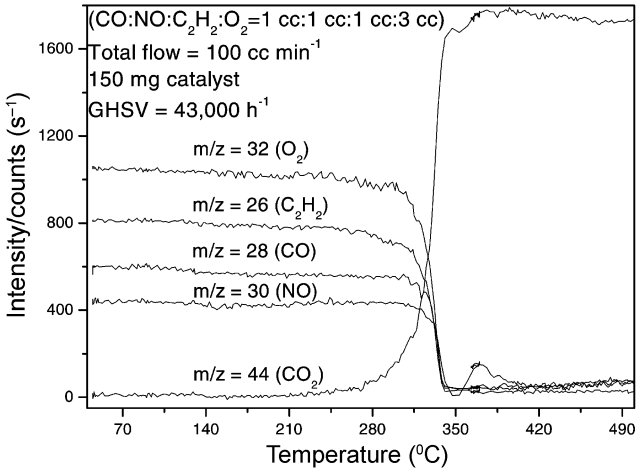

Figure 7. Total conversion of CO (10,000 ppm), NO (10,000 ppm), C_2H_2 (10,000 ppm) with 30,000 ppm of O_2 (15% excess oxygen) over 150 mg $Ce_{0·89}Pt_{0·01}La_{0·1}O_{1–d}$ catalyst at a space velocity of 43,000 h^{-1}.

higher over the La- and Y-substituted $Ce_{0·99}Pt_{0·01}O_{2–d}$ catalysts.

Three-way catalytic test is carried out by passing a simulated mixture of 1 ml of CO, 1 ml of C_2H_2 and 1 cc of NO with 3 cc of O_2 and the remaining 94 cc of He to make a total of 100 cc/min over 150 mg of $Ce_{0·89}Pt_{0·01}La_{0·1}O_{1–d}$ catalyst. With the volume of the catalyst bed of 0·139 cc, space velocity comes out to be 43,000 h^{-1}. The gas mixture contains 10,000 ppm of CO, 10,000 ppm of acetylene, 10,000 ppm of NO and 30,000 ppm of oxygen molecules in the flow. All the three pollutants at this impurity level are converted to CO_2, N_2 and water below 330°C, as can be seen from figure 7. The system therefore can be routinely used to test the exhausted catalysts. In this laboratory, ceria catalysts substituted with 2% Pd have been made and they show CO, NO and hydrocarbons catalytic conversion at temperatures below 200°C.

4. Conclusions

(i) A versatile temperature-programmed reaction system has been fabricated indigenously to study gas–solid heterogeneous catalytic reactions under realistic flow conditions.
(ii) The data acquisition system is efficient enough to record low concentrations at 5–10 ppm level and data processing is also very fast.
(iii) Lanthanum- and yttrium-substituted catalysts crystallize in fluorite structure with higher oxide-ion vacancy.
(iv) Formation of fixed oxide-ion vacancy on La/Y substitution increases the catalytic activity for CO oxidation.

Acknowledgements

MSH is grateful to Professor J Goplakrishnan for innumerable discussions in the broad area of solid state chemistry, which have helped the authors to come up with ionically substituted CeO_2 catalysts. Financial support from the Department of Science and Technology (DST), Government of India is gratefully acknowledged. AG is thankful to the Council of Scientific and Industrial Research (CSIR), Government of India, for a fellowship.

References

1. Cvettanovic R J and Anemenomia Y 1967 *Adv. Catal.* **17** 103
2. Jenkins J W 1975 *Gordon research conference on catalysis*, Colby-Sawyer College, New London, NH
3. Robertson S D, McNicol B D, De Bass J H, Kloet S C and Jenkins J W 1975 *J. Catal.* **37** 424
4. Dawson P T and Walker P C 1987 *Adv. Catal.* **36** 211
5. Jacobs P A, Linart J, Nijs H and Uyterhoeven J B 1977 *J. Chem. Soc. Faraday Trans. I* **73** 1745
6. Wagstaff N and Prins R J 1979 *J. Catal.* **59** 434
7. Lycourghiotis A, Defosse C, Delannay F, Lemaitre J and Delmon B J 1981 *J. Chem. Soc., Faraday Trans. I* **77** 603
8. Hurst N W, Gentry S J, Jones A and McNicol B D 1982 *Catal. Rev.-Sci. Eng.* **24** 233
9. Jones A and McNicol B D 1986 *Temperature-programmed reduction for solid materials characterization* (New York: Dekker)
10. Boer H, Boersma W J and Wagstaff N 1982 *Rev. Sci. Instrum.* **54** 349
11. Hegde M S, Ramesh S and Ramesh G S 1992 *Proc. Indian Acad. Sci.* (*Chem. Sci.*) **104** 591
12. Doraiswamy L K and Tajbl D G 1975 *Catal. Rev.* **10** 177
13. Thomas J M and Thomas W J 1967 *Introduction to the principles of heterogeneous catalysis* (London: Academic Press)
14. Bera P, Priolkar K R, Gayen A, Sarode P R, Hegde M S, Emura S, Kumashiro R, Jayaram V and Subbanna G N 2003 *Chem. Mater.* **15** 2049
15. Rodríguez-Carvajal J 2001 An introduction to the program FullProf 2000 (Version July 2001), Laboratoire Léon Brillouin (CEA-CNRS), CEA/Saclay, France
16. Bera P, Gayen A, Hegde M S, Lalla N P, Spadaro L, Frusteri F and Arena F 2003 *J. Phys. Chem.* **B107** 6122
17. Cao G, Seimiya Y, Ohno Y and Matsushima T 1998 *Chem. Phys. Lett.* **294** 419
18. Burwell R L Jr 1976 *Pure Appl. Chem.* **46** 71